TESTING AND SIMULATION OF CONTACT DURING ON-ORBIT OPERATIONS

Jakub Oleś [(1)], Tomasz Rybus [(1)], Karol Seweryn [(1)] , Marek Surowiec [(2)] , Marek Wojtyra [(2)] , Markus Pietras[(3)], Marc Scheper [(3)]

[(1)] Space Research Centre of the Polish Academy of Sciences (CBK PAN), Bartycka 18a, 00-716 Warsaw, Poland, Email: joles@cbk.waw.pl

[(2)] Institute of Aeronautics and Applied Mechanics, Warsaw University of Technology, Nowowiejska 24, 00-665, Warsaw, Poland

[(3)] OHB System AG, Universitätsallee 27-29, 28359 Bremen, Germany

ABSTRACT

Capabilities for capturing objects on Earth's orbit by unmanned satellites are required in the planned On-Orbit Servicing and Active Debris Removal missions. The majority of proposed mission concepts relies on the use of manipulator for on-orbit capture. Behaviour of the system during contact of the gripper with the target object requires special attention. Contact is a highly nonlinear phenomenon and it is difficult to obtain high fidelity models of contact. This paper presents approach to investigate the contact phase of the on-orbit capture manoeuvre in experiments with scaled down system on the planar air-bearing microgravity simulator. We propose to use gripper mock-up that does not have the same functionality as the nominal gripper, but is relevant in terms of contact parameters.

1. INTRODUCTION

Capabilities for capturing objects on Earth's orbit by unmanned satellites are required in the planned On-Orbit Servicing (OOS) and Active Debris Removal (ADR) missions. The purpose of the proposed OOS missions is to prolong operational lifetime of Earth-orbiting satellites by performing on-orbit servicing operations such as refuelling and replacement of broken components [1], while the purpose of ADR missions is to capture and remove from orbit large space debris in order to prevent growth of debris population [2]. The majority of mission concepts, that were proposed in recent years, relies on the use of a manipulator for performing on-orbit capture manoeuvre (e.g., [3], [4]). Use of a manipulator is also considered as a baseline solution in the e.Deorbit mission [5]. This mission is currently being prepared by the European Space Agency (ESA) to demonstrate technologies required for ADR by removing one large defunct satellite from orbit (ESA's satellite Envisat was selected as a target for this demonstration).

The grasping phase will be the most challenging part of OOS and ADR missions due to reasons such as: the required high autonomy, the influence of the manipulator motion on the state of the manipulator-equipped chaser satellite, a high risk of collision, and problems with prediction of system's behaviour during contact between the gripper mounted on the manipulator arm and the target object. Detailed numerical simulations of the grasping manoeuvre are very difficult and time consuming. Such simulations should include an orbital motion of the chaser (described as a multibody system) and the target satellite, operations of the Guidance, Navigation, and Control (GNC) subsystems of the chaser satellite and control subsystem of the manipulator, as well as contact between the gripper and the selected fixture on the target object. Contact is a highly nonlinear phenomenon and it is difficult to obtain high fidelity models of contact. There are only several studies focused on the numerical simulations of contact during the grasping manoeuver performed with the use of a manipulator arm (e.g., results of contact dynamics simulation for an unmanned servicing mission to the Hubble Space Telescope can be found in [6]). As stated in [7], managing the contact dynamics between a robotic servicing vehicle and a target object is one of the most fundamental capabilities required to enable OOS and ADR missions. Various approaches for control can be used during the contact phase [8]. Notable examples include the control strategy based on impedance matching that is proposed in [9] and the control system based on a combination of resolved motion rate control method and admittance control technique that is presented in [10].

Due to difficulties in modelling contact, ground experiments are required to validate numerical models [11]. However, such experiments are challenging as they require simulations of microgravity environment. Moreover, because the size of the test facilities is limited, experiments must be performed with mock-ups that are scaled down. To obtain the same dynamic behaviour of the scaled system the mass and inertia of all components must be scaled [12]. Furthermore, the material properties of the contacting bodies should also be changed. Two kinds of facilities seem especially suitable for the experiments related to contact dynamics in the context of orbital capture manoeuvers: planar air-bearing microgravity simulators [13] and facilities based on industrial robots that simulate motion of the chaser and the target satellite (such as platform-art operated by

GMV [14] and EPOS operated by DLR [15]). Results related to contact dynamics obtained with the first method can be found in [16] and [17], while results obtained with the second method can be found in [18] and [19]. Experimental results obtained during simulation of the capture manoeuver performed with the WMS2 LEMUR manipulator on the platform-art facility are shown in [20]. In the performed experiments algorithm based on the impedance control was used during the contact phase.

This paper presents an approach to investigate the contact phase of the on-orbit capture manoeuvre in experiments with scaled down system on the planar air-bearing microgravity simulator at the Space Research Centre (CBK PAN) [21]. Scenario considered in the main part of this paper is based on the proposed e.Deorbit mission, in which gripper is used to grasp the Launch Adapter Ring (LAR) of the Envisat [22]. A set of 27 tests was performed on the test-bed. Test campaign was supplemented by numerical simulations required to predict behaviour of the gripper during experiments with various initial conditions. To perform numerical simulations the 'Simulation tool for space robotics', that was developed at the CBK PAN, was upgraded with MSC ADAMS module simulating contact between the gripper and the LAR. The tests and simulations have shown difficulties in capturing with the full scale gripper mock-up. Therefore, we propose a new approach to contact investigation. Especially, we propose to develop a modified version of gripper for possible future tests and provide simulations of capturing the LAR. In the presented approach we use a simplified model of contact that is based on elastic-plastic point objects interactions.

The paper is organized as follows. Theoretical model of the capture manoeuver is presented in Section 2. The selected approach towards scaling down of the orbital system is described in Section 3. along with results of numerical simulations and tests, while the new experimental test set-up is presented in Section 4. Conclusions are provided in Section 5.

2. THEORETICAL MODEL

In this section, equations for the general case of spatial *n*-DoF manipulator (with rotational joints) mounted on the chaser satellite are introduced. These equations are derived without the assumption of zero momentum and angular momentum so might be applied for the final phase of chaser motion where its control system is synchronizing the motion to keep constant state with respect to the target satellite. We follow the approach presented in [23] and [24]. Geometrical parameters and coordinate systems of the satellite-manipulator system are shown in Fig. 1. Equations presented in this section are expressed in the inertial reference frame CS_{ine}.

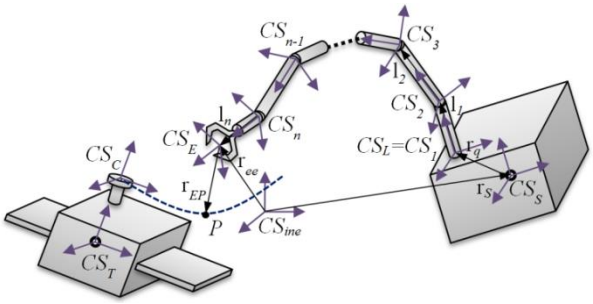

Fig. 1 Schematic view of the satellite-manipulator system

Position of the manipulator end effector (EE) is given as:

$$\mathbf{r}_{ee} = \mathbf{r}_s + \mathbf{r}_q + \sum_{i=1}^{n} \mathbf{l}_i \qquad (1)$$

where $\mathbf{r}_s$ is the position of the servicing satellite center of mass (CM), $\mathbf{r}_q$ is the position of the first kinematic pair of the manipulator with respect to the satellite (given in CS_{ine}), and $\mathbf{l}_i$ is the position of the $(i+1)$th kinematic pair with respect to the ith kinematic pair (also given in CS_{ine}). Linear velocity of the EE is expressed as:

$$\mathbf{v}_{ee} = \mathbf{v}_s + \boldsymbol{\omega}_s \times (\mathbf{r}_{ee} - \mathbf{r}_s) + \sum_{i=1}^{n} [\mathbf{k}_i \times (\mathbf{r}_{ee} - \mathbf{r}_i)]\dot{\theta}_i \qquad (2)$$

where $\mathbf{v}_s$ and $\boldsymbol{\omega}_s$ are the linear and angular velocity of the servicing satellite, respectively, $\mathbf{k}_i$ and $\mathbf{r}_i$ are the unit vector of angular velocity and position of the ith kinematic pair, respectively, while $\dot{\theta}_i$ is the first derivative with respect to time of the position of ith rotational joint and denotes the angular velocity of this joint. The angular velocity of the EE can be expressed through angular velocities of the satellite and of the kinematic pairs:

$$\boldsymbol{\omega}_{ee} = \boldsymbol{\omega}_s + \sum_{i=1}^{n} \mathbf{k}_i \dot{\theta}_i \qquad (3)$$

The EE linear and angular velocity can be expressed using vector notation:

$$\begin{bmatrix} \mathbf{v}_{ee} \\ \boldsymbol{\omega}_{ee} \end{bmatrix} = \mathbf{J}_s \begin{bmatrix} \mathbf{v}_s \\ \boldsymbol{\omega}_s \end{bmatrix} + \mathbf{J}_M \dot{\boldsymbol{\theta}} \qquad (4)$$

where $\mathbf{J}_S$ is the Jacobian of the satellite, $\mathbf{J}_M$ is the Jacobian of the manipulator, while vector $\dot{\boldsymbol{\theta}}$ contains angular velocities of manipulator joints. For the general spatial case Jacobian of the satellite is given by the following 6 x 6 matrix:

$$\mathbf{J}_s = \begin{bmatrix} \mathbf{I} & \tilde{\mathbf{r}}_{ee\_s}^{T} \\ \mathbf{0} & \mathbf{I} \end{bmatrix} \qquad (5)$$

where $\mathbf{r}_{ee\_s} = \mathbf{r}_{ee} - \mathbf{r}_s$, $\mathbf{I}$ is the identity matrix, $\mathbf{0}$ denotes the zero matrix and symbol ~ denotes matrix, which is equivalent to a vector cross-product. $\mathbf{J}_M$ in Eq. (4) is a standard Jacobian of a fixed-base manipulator expressed in CS_{ine}. It is a 6 x n dimensional matrix:

$$\mathbf{J}_M = \begin{bmatrix} \mathbf{k}_1 \times (\mathbf{r}_{ee} - \mathbf{r}_1) & \cdots & \mathbf{k}_n \times (\mathbf{r}_{ee} - \mathbf{r}_n) \\ \mathbf{k}_1 & \cdots & \mathbf{k}_n \end{bmatrix} \quad (6)$$

The kinetic energy of the satellite-manipulator system can be expressed as:

$$\mathbf{T} = \frac{1}{2} \begin{bmatrix} \mathbf{v}_s \\ \boldsymbol{\omega}_s \\ \dot{\boldsymbol{\theta}} \end{bmatrix}^T \begin{bmatrix} \mathbf{A} & \mathbf{B} & \mathbf{D} \\ \mathbf{B}^T & \mathbf{E} & \mathbf{F} \\ \mathbf{D}^T & \mathbf{F}^T & \mathbf{N} \end{bmatrix} \begin{bmatrix} \mathbf{v}_s \\ \boldsymbol{\omega}_s \\ \dot{\boldsymbol{\theta}} \end{bmatrix} \quad (7)$$

where the submatrices **A**, **B**, **D**, **E**, **F** and **N** are defined in [23]. The angular momentum of the satellite manipulator system is given by the following equation:

$$\mathbf{L} = \mathbf{L}_0 + \mathbf{r}_s \times \mathbf{P} \quad (8)$$

where $\mathbf{L}_0$ denotes the initial angular momentum. The momentum **P** and the angular momentum of the system can be expressed as:

$$\begin{bmatrix} \mathbf{P} \\ \mathbf{L}_0 + \mathbf{r}_s \times \mathbf{P} \end{bmatrix} = \mathbf{H}_2 \begin{bmatrix} \mathbf{v}_s \\ \boldsymbol{\omega}_s \end{bmatrix} + \mathbf{H}_3 \dot{\boldsymbol{\theta}} = \begin{bmatrix} \mathbf{f}_m \\ \mathbf{f}_{am} \end{bmatrix} \quad (9)$$

where:

$$\mathbf{H}_2 = \begin{bmatrix} \mathbf{A} & \mathbf{B} \\ \mathbf{B}^T + \tilde{\mathbf{r}}_s \mathbf{A} & \mathbf{E} + \tilde{\mathbf{r}}_s \mathbf{B} \end{bmatrix} \quad (10)$$

$$\mathbf{H}_3 = \begin{bmatrix} \mathbf{D} \\ \mathbf{F} + \tilde{\mathbf{r}}_s \mathbf{D} \end{bmatrix} \quad (11)$$

The momentum and angular momentum of the satellite manipulator system are not conserved. They depend on the forces $\mathbf{F}_s$ and torques $\mathbf{H}_s$ acting on the satellite (we assume that these forces and torques are known *a priori*). The functions: $\mathbf{f}_m = \int \mathbf{F}_s dt$ and $\mathbf{f}_{am} = \int \mathbf{H}_s + \tilde{\mathbf{r}}_s \mathbf{F}_s dt$ in Eq. (9) describe changes of momentum and angular momentum. This approach allow us to take into account the forces and torques induced by the control system responsible for controlling position and orientation of the satellite. However, satellite control system was not used in the tests that were performed up to now.

The relation between the EE velocity and velocities of manipulator joints can be expressed as:

$$\begin{bmatrix} \mathbf{v}_{ee} \\ \boldsymbol{\omega}_{ee} \end{bmatrix} = \mathbf{J}_s \mathbf{H}_2^{-1} \begin{bmatrix} \mathbf{f}_m \\ \mathbf{f}_{am} \end{bmatrix} + \left(\mathbf{J}_M - \mathbf{J}_s \mathbf{H}_2^{-1} \mathbf{H}_3 \right) \dot{\boldsymbol{\theta}} \quad (12)$$

The Eq. (12) can be transformed to obtain the following expression for velocities of manipulator joints:

$$\dot{\boldsymbol{\theta}} = \left(\mathbf{J}_M - \mathbf{J}_s \mathbf{H}_2^{-1} \mathbf{H}_3 \right)^{-1} \left(\begin{bmatrix} \mathbf{v}_{ee} \\ \boldsymbol{\omega}_{ee} \end{bmatrix} - \mathbf{J}_s \mathbf{H}_2^{-1} \begin{bmatrix} \mathbf{f}_m \\ \mathbf{f}_{am} \end{bmatrix} \right) \quad (13)$$

The servicing satellite velocity is given by:

$$\begin{bmatrix} \mathbf{v}_s \\ \boldsymbol{\omega}_s \end{bmatrix} = \mathbf{H}_2^{-1} \left(\begin{bmatrix} \mathbf{f}_m \\ \mathbf{f}_{am} \end{bmatrix} - \mathbf{H}_3 \dot{\boldsymbol{\theta}} \right) \quad (14)$$

Angular velocity of the servicing satellite, $\boldsymbol{\omega}_s$, determines, through kinematic equations, the transformation matrix between the CS_{ine} and the body fixed coordinate system (CS_S).

To derive dynamics equations for the satellite-manipulator system we use Langrangian formalism. Considering relative several meters spacecraft motion in the orbital environment the potential energy might be neglected. In such a case the generalized coordinates were chosen in the following form:

$$\mathbf{q}_p = [\mathbf{r}_s{}^T \quad \boldsymbol{\Theta}_s{}^T \quad \boldsymbol{\theta}^T]^T \quad (15)$$

$$\mathbf{q}_v = [\mathbf{v}_s{}^T \quad \boldsymbol{\omega}_s{}^T \quad \dot{\boldsymbol{\theta}}^T]^T \quad (16)$$

where $\boldsymbol{\Theta}_s$ is the vector containing Euler angles that describe the orientation of the servicing satellite. The generalized equations of motion for the satellite equipped with a non-redundant 6 DoF manipulator can be expressed as:

$$\mathbf{M}(\mathbf{q}_p)\ddot{\mathbf{q}}_p + \mathbf{C}(\dot{\mathbf{q}}_p, \mathbf{q}_p)\dot{\mathbf{q}}_p = \begin{bmatrix} \mathbf{F}_s \\ \mathbf{H}_s \\ \mathbf{u}_{ref} + \mathbf{u}_{contr} \end{bmatrix} + \begin{bmatrix} \mathbf{J}_S \\ \mathbf{J}_M \end{bmatrix} \begin{bmatrix} \mathbf{F}_{ee} \\ \mathbf{T}_{ee} \end{bmatrix} \quad (17)$$

where **M** is defined as:

$$\mathbf{M} = \begin{bmatrix} \mathbf{A} & \mathbf{B} & \mathbf{D} \\ \mathbf{B}^T & \mathbf{E} & \mathbf{F} \\ \mathbf{D}^T & \mathbf{F}^T & \mathbf{N} \end{bmatrix} \quad (18)$$

while components of **C** matrix are computed using algorithms dedicated to quasi coordinates. The $\mathbf{F}_{ee}$ and $\mathbf{T}_{ee}$ is a force and torque generated at the EE for example due to contact with the target body. For a given reference control torques $\mathbf{u}_{ref}$ (computed in the trajectory planning phase) and without disturbances the system realize reference trajectory. In case of disturbances the control system must generate torques $\mathbf{u}_{contr}$ that will reduce the EE position error to zero.

3. APPROACH TOWARD SCALING DOWN

3.1. Tests and simulations based on the e.Deorbit mission

The tests and simulations of capturing based on the e.Deorbit mission were performed for a scaled down chaser satellite and target satellite. It would be extremely difficult to test a full-scale model of Envisat due to manufacturing costs and limited capabilities of the testing facility. Therefore, scaling laws were used to obtain a mock-up that could fit on the microgravity simulator in CBK PAN. An approach with scaling laws is often used to achieve valuable test results of mock-ups with lower size and weight [12]. The results from such a test can be re-scaled to full scale model and used for proper analysis. The main formula for the scaling law is presented in Eq. (19).

$$\mathrm{P_s} = \lambda^{\mathrm{w}} \mathrm{P} \quad (19)$$

where: P_s – value after scaling, λ – scaling coefficient, w – scaling exponent, P – value before scaling. Several exemplary scaling exponents are shown in Tab. 1. A schematic view of the scaled down experimental test set-up is shown in Fig. 2. The experiments included free-floating chaser satellite with planar 2 DoF manipulator and free-floating target satellite. The

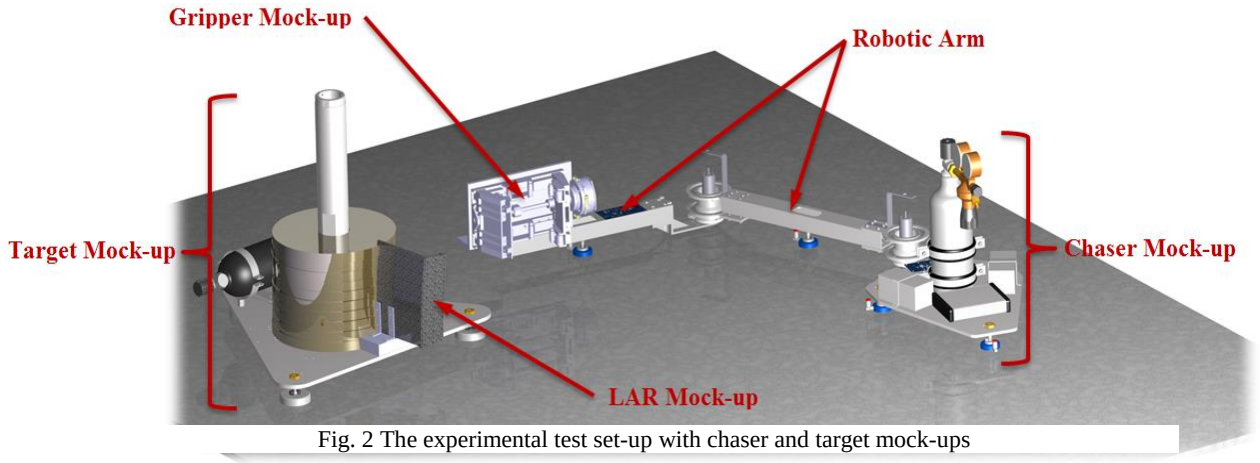

Fig. 2 The experimental test set-up with chaser and target mock-ups

contact forces occurring during grasping influenced position and orientation of both objects. The experiments were performed with the scaling coefficient λ=0.3.The parameters before and after scaling are shown in Tab. 2 and mock-ups' parameters in simulations and tests are shown in Tab. 3.

Tab. 1 Exemplary scaling exponents commonly used in scaling laws

Physical property	**Scaling exponent**	**Physical property**	**Scaling exponent**
Distance	1	Inertia	5
Time	1	Velocity	0
Frequency	-1	Acceleration	-1
Force	2	Energy	3
Mass	3	Power	2
Stiffness	1	Damping	2

Tab. 2 Parameters of nominal and scaled system with scaling coefficient λ=0.3

Parameter	**Nominal 3D case**	**After scaling**
Target mass [kg]	7900	213.3
Target inertia [kg*m^2]	129112.2	313.7
Chaser mass [kg]	1500	40.5
Chaser inertia [kg*m^2]	762	1.85
Robotic arm length [m]	4.2	1.26
Gripper stroke [cm]	7	2.1
Time of gripping [s]	5	1.5

Tab. 3 Parameters of system in tests and simulations

Parameter	**Tests**	**Simulations**
Target mass [kg]	~ 200	200
Target inertia [kg*m2]	~ 4.81	4.81
Chaser mass [kg]	~ 40	43.8
Chaser inertia [kg*m2]	1.40	1.61
Robotic arm length [m]	1.26	1.26
Gripper stroke [cm]	7	7
Time of gripping [s]	5	4-5

The goal of simulation activity was to predict behavior of gripper on the microgravity simulator during tests so the parameters used in the activity were chosen to be similar to parameters of test system.

The gripper was not scaled down because it would lead to major complications in the design and the scaled gripper would have an extremely small stroke. Also, required linear misalignments (+-20 mm) would be scaled to 6 mm which would be difficult to obtain with sufficient precision during tests without a professional positioning system. The proper inertia of the target satellite is also very problematic to achieve due to limited space on the microgravity simulator compared to both the nominal dimensions of Envisat (26 m x 10 m x 5 m) and the dimensions after scaling (7.8 m x 3.3 m x 1.5 m). The mass of the target mock-up has to be concentrated in a little space and therefore it is impossible to achieve correct inertia through proper mass distribution.

As stated in Introduction, experiments described in this paper were performed on the planar air-bearing microgravity simulator at CBK PAN [21]. The main element of this test-bed is a 2 m x 3 m granite table, flat and precisely levelled. Mock-up of the manipulator-equipped chaser satellite and mock-up of the target satellite are mounted on planar air-bearings. Almost frictionless motion on the table surface is provided by these air-bearings. Thus, microgravity conditions are simulated in two dimensions (the motion is limited to one plane). During experiments chaser satellite is in a free-floating state [25] and motion of the manipulator is controlled in the configuration space by a control system implemented on the chaser mock-up on-board computer. Bluetooth is used for communication between the on-board computer and PC master (placed outside the granite table) to avoid disturbances in the chaser motion that might by caused by a cable connection. An external vision system based on two industrial cameras mounted above the table surface is used to track position and orientation of all objects on the test-bed.

The tests and simulations were performed for various initial conditions which included initial position of the gripper mock-up being moved by a distance of 20 mm in both x and y directions with respect to the LAR and initial orientation tilted by 5 deg (some tests were performed with bigger angular misalignment). However, there was no relative velocity between the chaser and the target. A schematic picture of initial position and correct final position is shown in Fig. 3. The gripper jaws (blue) are mounted on a single spindle with right and left thread and actuated by one motor. The green carriages are held in initial position by springs. Red rollers are intended for contact with the LAR. The gripper, especially the carriages, close passively because of the jaws actuation and forces resulting from the contact with the LAR. A model of RoboDriveILM 70x18 was implemented to actuate the gripper jaws.

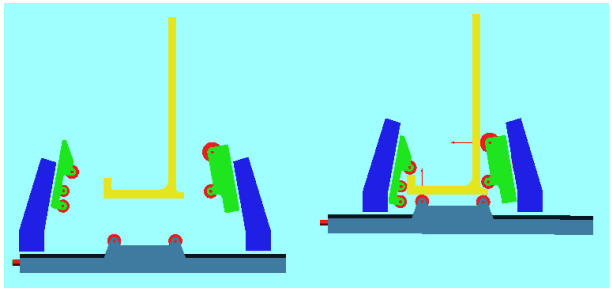

Fig. 3 Initial and correct final position of the LAR

The contact force in MSC ADAMS contact module was modeled as spring-damper interaction. The parameters were chosen to have stable integration of equations. Friction between parts of the gripper was not modeled in ADAMS. Especially, friction between rollers and pins, friction between movable parts of jaws and friction between rollers and the LAR was neglected. The contact parameters used in simulations in MSC ADAMS are shown in Tab. 4.

Tab. 4 Contact parameters in MSC ADAMS contact module

Parameter	**Range**
Stiffness between the LAR and each roller on the gripper	5.0^4 - 1.0^6 N/m
Damping between the LAR and each roller on gripper	1.0^5 - 1.0^8 Ns/m
Spring stiffness between the movable part of jaws	20 – 100 N/m
Spring damping between the movable part of jaws	10 – 1000 Ns/m

The simulation activity has shown that correct gripping is very difficult to achieve. Two common final positions are presented in Fig. 4. The outline of simulation activity is shown in Tab. 5.

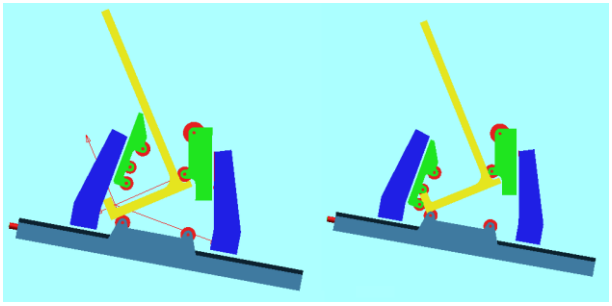

Fig. 4 Final positions in simulation: A – on the left, B – on the right

Tab. 5 Simulation results for various initial orientation misalignments (Δθ) and linear misalignments in *x* axis (Δx) and *y* axis (Δy)

Δθ = 0 deg	**Δx= -20 mm**	**Δx = 0 mm**	**Δx = 20 mm**
Δy= -20 mm	A	A	A
Δy = 0 mm	A	A	A
Δy = 20 mm	B	A	A
Δθ = -5 deg	**Δx= -10 mm**	**Δx = 0 mm**	**Δx = 10 mm**
Δy= -10 mm	A	A	A
Δy = 0 mm	B	B	A
Δy = 10 mm	B	B	B
Δθ = 0 deg	**Δx= -10 mm**	**Δx = 0 mm**	**Δx = 10 mm**
Δy= -10 mm	A	A	A
Δy = 0 mm	A	A	A
Δy = 10 mm	B	A	A

The tests also have shown that the gripper has a tendency to catch the LAR and then rotate, as presented in Fig. 5. Final positions of the system during tests can be classified into two groups, presented in Fig. 6. Test results of the tests are outlined in Tab. 6.

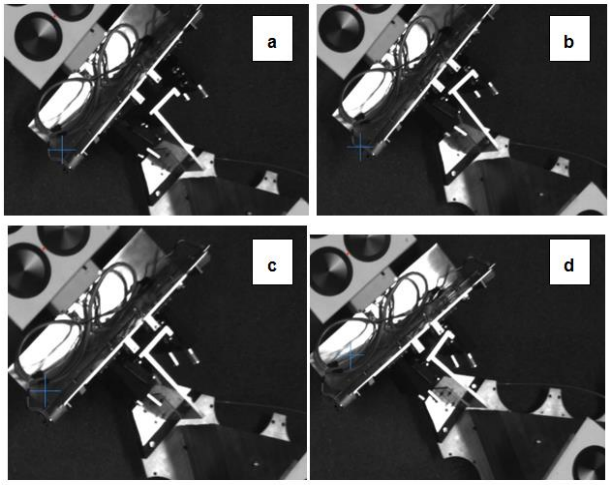

Fig. 5 Results from the tests on air-bearing microgravity simulator

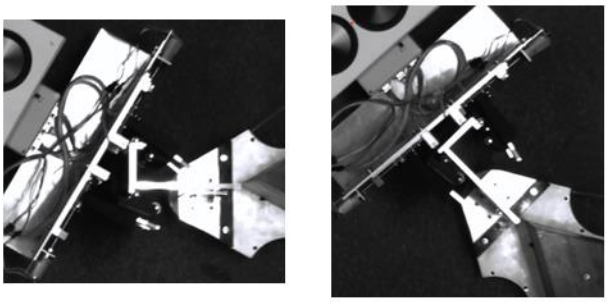

Fig. 6 Final positions during tests on the air-bearing microgravity simulator: B – on the left, C – on the right

Tab. 6 Results of tests performed on the planar air-bearing simulator

Δθ = 0 deg	**Δx= -20 mm**	**Δx = 0 mm**	**Δx = 20 mm**
Δy= -20 mm	B	B	B
Δy = 0 mm	B	B	B
Δy = 20 mm	C	B	C
Δθ = -5 deg	**Δx= -20 mm**	**Δx = 0 mm**	**Δx = 20 mm**
Δy= -20 mm	B	C	B
Δy = 0 mm	B	B	B
Δy = 20 mm	B	C	B
Δθ = 0 deg	**Δx= -20 mm**	**Δx = 0 mm**	**Δx = 20 mm**
Δy= -20 mm	B	B	B
Δy = 0 mm	B	B	B
Δy = 20 mm	B	B	B

The rotation of the LAR during gripping was observed in both simulations and tests. However, in simulation the process was more dynamic, as shown in Fig. 7.

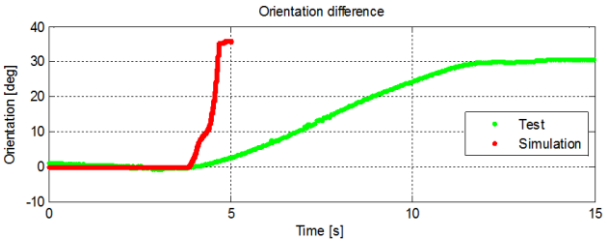

Fig. 7 The rotation of the LAR with respect to the gripper in test and corresponding simulation

During tests a significant friction was observed between the carriages and jaws. Also, the motors used in the gripper design (due to manufacturing costs a solution with 2 separate motors for each jaw was chosen) should be more powerful. However, it could lead only to faster rotation of the target mock-up. These issues might have influenced the test results, but there could be several another reasons, especially concerning the fact, that the system was not scaled down precisely. What is the most significant, the gripper and the LAR were not scaled at all and the target inertia differed significantly from the desired value.

The facts that nor simulation neither test activity was successful and that the results from simulations and tests proved to be comparable led to a new approach to the contact investigation, which is presented in the following sections.

3.2. The concept of a simplified gripper

The new approach is based on more accurate scaling of the system. In order to present the approach, a simulation model with a simplified gripper was made. A behavior of the model with simplified contact module (SIM2) was compared and tuned to represent full scale 2D model with a modified ADAMS MSC gripper (SIM1), shown previously in Section 3.1. The modifications in SIM1 consisted of the introduction of two operation modes of the gripper:

- Soft contact: the carriages can move without much resistance with respect to the jaws. The mode represent initial phase of capturing.
- Rigidization: the carriages and jaws are in a closed position and their movement is restricted. Therefore, the LAR is held firmly in a correct final position.

The contact in SIM2 is based on the elastic-plastic interactions. In this approach, the contact force is calculated as a sum of the elastic component, proportional to the distance δ, and the plastic component proportional to the relative velocity (Fig. 8).

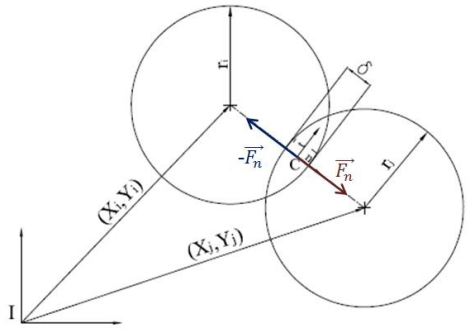

Fig. 8 Point elastic-plastic interactions contact model

The force is given by:

$$F_n = k \cdot \delta + \eta_n \cdot v_n \cdot \theta(v_n) \qquad (20)$$

where: F_n – normal force [N], k – stiffness, proportional to Young's modulus, δ – difference of the distance between the centers of mass of the two objects and the sum of their radii $(r_i + r_j)$ [m], η_n – damping coefficient, v_n – relative velocity [m/s], θ – Heaviside function. The Heaviside function activates the plastic component of the force when the objects are approaching each other. It therefore acts as a damping factor which reduces oscillations produced by the elastic part. The gripper itself is modelled as three balls: P1 (red) – located on EE, and movable P1(yellow) and P2 (green) – representing gripper jaws. The docking port T1(blue) represents the LAR. The gripping process is shown in Fig. 9.

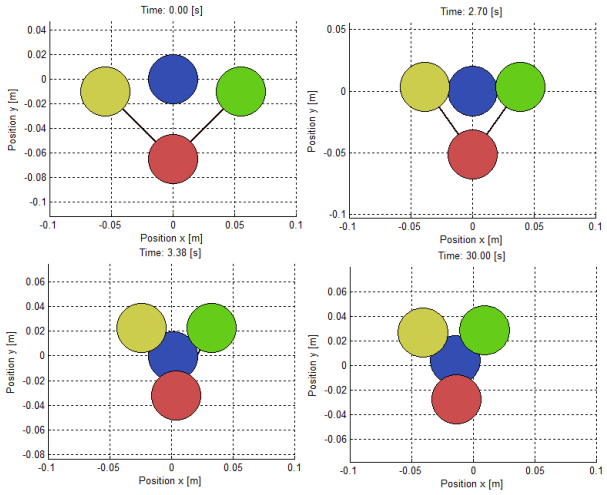

Fig. 9 Capturing with simplified gripper in SIM2

The parameters used in SIM1 and SIM2 are shown in Tab. 7. Simulation SIM2 was then used as a reference for scaling in SIM3 which is described in Section 3.3.

Tab. 7 Simulation parameters

Parameter	**SIM1 / SIM2**	**SIM3**
Target mass [kg]	7900	213.3
Target inertia [kg*m^2]	129112.2	313.7
Chaser mass [kg]	1720	46.4
Chaser inertia [kg*m^2]	762	1.85
Distance from the LAR mounting point to target CoG [m]	[5.0, 1.3]	[1.5, 0.39]
Robotic arm mass [kg]	58.7	1.6
Robotic arm length [m]	2.12	0.63
Stiffness k [N/m]	20000 (SIM2)	6000
Damping η_n [Ns/m]	900 (SIM2)	81
Initial velocity between chaser and target [m/s]	0.005	0.005
Time of simulation [s]	30	10

The simulations performed in SIM1 and SIM2 are comparable to each other in terms of kinetic energy of target and gripper parts with respect to the EE (gripper mounting point on the manipulator arm). During the maneuver only the capturing is investigated so the manipulator holds its configuration (does not perform any trajectory in configuration space) and the energy of links is equal to zero. In order to calculate the kinetic energy, relative velocities of the target and the moving parts of the gripper were found:

$$\mathbf{v}_{i\_ee} = \mathbf{v}_{IN\_i} - (\mathbf{v}_{ee} - \boldsymbol{\omega}_{ee} \times \boldsymbol{r}_i) \qquad (21)$$

where: $\mathbf{v}_{i\_ee}$ – velocity of the component with respect to the EE, $\mathbf{v}_{IN\_i}$ – velocity of the component in the inertial frame, $\mathbf{v}_{ee}$ – velocity of the EE in the inertial frame, $\boldsymbol{\omega}_{ee}$ – angular velocity of the EE in the inertial frame, $\boldsymbol{r}_i$ – vector from the EE to a component.

The kinetic energy in the EE reference frame is formulated:

$$E_{kin\_EE} = \left(\sum_{i=1}^{n} m_i \, {v_{i\_ee\_n}}^2 + I_{i\_z} \left(\omega_{i\_z} - \omega_{ee\_z} \right)^2 \right) / 2 \qquad (22)$$

where: m_i – mass of a component, $v_{i\_ee\_n}$ – norm of the vector $\mathbf{v}_{i\_ee}$, I_{i_z} – inertia with respect to the axis z (perpendicular to the plane of motion) crossing the center of mass of a component, ω_{i_z} – angular velocity of a component with respect to z axis, ω_{ee_z} – angular velocity of the EE with respect to z axis. The contact parameters in SIM2 were tuned as to come up with similar energy graph (Fig. 10).

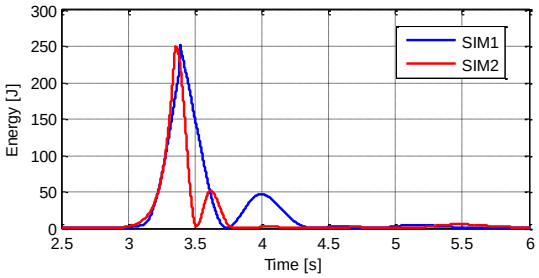

Fig. 10 Energy in simulations SIM1 and SIM2

3.3. Simulations of a scaled down system

Parameters of simulation SIM2 were scaled down with a scaling coefficient λ=0.3. Scaling included not only physical properties, like dimensions and mass, but also contact parameters. The reason is that in order to obtain the same dynamic behaviour of the scaled system the material properties of the contacting bodies should also be changed. From the selected model of contact Eq. (**23)** and from the scaling law it arises that for the stiffness k, the scaling exponent $w1$ = 1, while for the damping coefficient η_n, the scaling exponent $w2$ = 2:

$$\lambda^2 \cdot F_n = \lambda^{w1} \cdot k \cdot \lambda^1 \cdot \delta + \lambda^{w2} \cdot \eta_n \cdot \lambda^0 \cdot v_n \cdot \theta(v_n) \qquad (23)$$

Thus, for the experimental set-up that is scaled down, the materials used for the contacting surfaces (gripper jaws and the LAR) should have lower stiffness (proportionally to the scaling factor of physical dimensions) and lower damping coefficient (proportionally to the square of scaling coefficient λ). The numerical simulations show that the selection of proper material properties is required to obtain high fidelity of experiments. Parameters of simulation SIM3 along with scaled stiffness and damping are shown in Tab. 7. The kinetic energy with respect to the EE of the scaled system in simulation SIM3 is shown in Fig. 11.

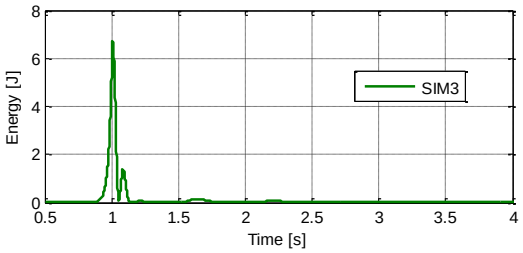

Fig. 11 Energy in simulation SIM3

It can be shown, that after rescaling with inverse scaling law, the results from SIM3 match simulation SIM2 (Fig. 12). Magnitudes of forces appearing on balls P1, P2 and P3 are shown in Fig. 13. Forces from SIM3 can be also rescaled to match values received in SIM2.

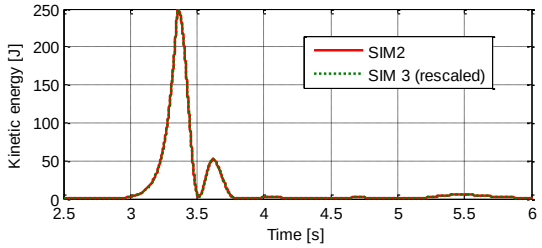

Fig. 12 Energy in simulation SIM2 and scaled up energy in simulation SIM3

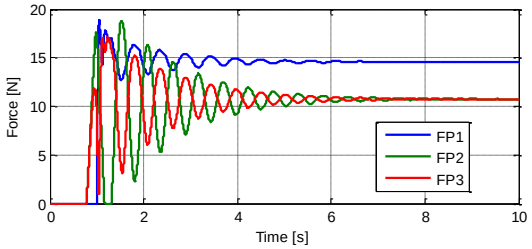

Fig. 13 Magnitudes of forces on P1, P2, P3 in simulation SIM3

4. EXPERIMENTAL TEST SET-UP BASED ON THE PLANAR AIR-BEARING MICROGRAVITY SIMULATOR

For the next experimental campaign several modifications were introduced to the chaser satellite mock-up. The mock-up, after modifications, is shown in Fig. 14, while details are provided in [21]. Set of 8 cold-gas thrusters was added to the mock-up for control of chaser position and orientation. Cold-gas thrusters will allow simulations of the chaser approach phase and experiments with full control of chaser motion during the grasping phase. In the next experimental campaign we propose to use a gripper mock-up that does not have the same functionality as the nominal gripper, but is relevant in terms of contact parameters (stiffness, damping), which are consistent with the scaling of the system (Fig. 15).

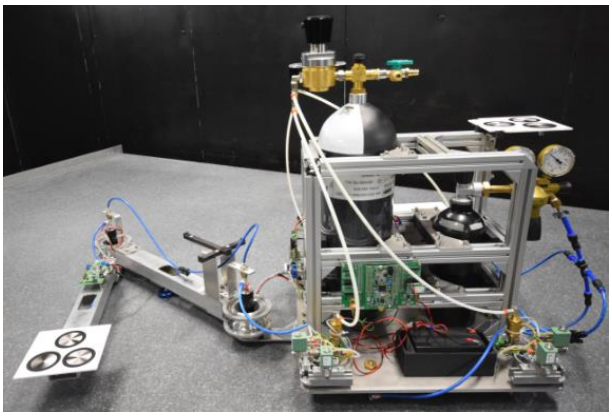
Fig. 14 The new chase satellite mock-up

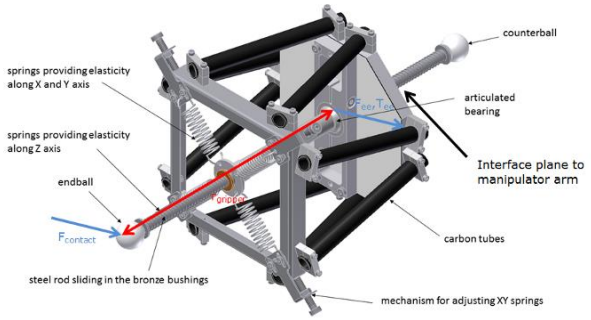

Fig. 15 The gripper dummy

The EE position is a reference position of the manipulator arm last link and it is also an interface point to the manipulator gripper. The end ball center is the reference position of dummy gripper and a surface of the end ball is a contact surface on the target satellite. The end ball is elastically mounted with respect to EE interface providing well defined flexibility and dumping (parameters estimated in previous sections). As an effect, the contact force $\mathbf{F}_{contact}$ generates the force $\mathbf{F}_{ee}$ and torque $\mathbf{T}_{ee}$ acting on the EE reference point. This force is treated as a main disturbance on the system. The end ball allows to transmit pulling and pushing force during contact. The goal of a manipulator arm control system is to keep contact force amplitude during the time estimated according to scaling laws.

5. CONCLUSIONS

The presented approach to perform the analysis of contact between gripper mounted on the manipulator EE (chaser satellite) and the LAR (part of the target satellite) can be summarized as follows:

- In the numerical simulations the scaled down parameters can be used assuming proper scaling of stiffness, damping gripper size and time of gripper closing.
- In the tests on the air-bearing table the dummy gripper can be used with control system set to keep contact with specific value of normal force between end ball and target plate.

6. ACKNOWLEDGMENTS

This paper was partially supported by The National Centre for Research and Development project no. PBS3/A3/22/2015 and e.Deorbit Phase B1 Study 4000114800/15/NL/GLC/CBK.

7. REFERENCES

1. Ellery, A., Kreisel, J., & Sommer, B. (2008). The case for robotic on-orbit servicing of spacecraft: spacecraft reliability is a myth. Acta Astronautica 63(5), 632-648.
2. Liou, J.-C., Johnson, N.L., & Hill, N.M. (2010). Controlling the growth of future LEO debris populations with active debris removal. Acta Astronautica 66(5-6), 648-653.
3. Yasaka, T. & Ashford, W. (1996). GSV: An Approach Toward Space System Servicing. Earth Space Review 5(2), 9-17.
4. Bischof, B., Kerstein, L., Starke, J., Guenther, H., Foth, W.-P., et al. (2003). ROGER – Robotic Geostationary Orbit Restorer. In: Proc of the 54th International Astronautical Congress, Bremen, Germany.
5. Biesbroek, R., Soares, T., Husing, J., & Innocenti, L. (2013). The e.Deorbit CDF Study: A Design Study for the Safe Removal of a Large Space Debris. In: Proc of the 6th European Conference on Space Debris, Darmstadt, Germany.
6. Wang, J., Mukherji, R., Ficocelli, M., Ogilvie, A., & Rice, C. (2006). Contact dynamics simulations for robotic servicing of Hubble Space Telescope. In: Motaghedi, P. (ed.) Modeling, Simulation, and Verification of Space-based Systems III. Proc. of SPIE vol. 6221.
7. Henshaw, C. & Tasker, F. (2008). Managing contact dynamics for orbital robotic servicing missions. In: Proc. of the AIAA SPACE 2008 Conference & Exposition, San Diego, California, USA.
8. Flores-Abad, A., Ma, O., Pham, K., & Ulrich, S. (2014). A review of space robotics technologies for on-orbit servicing. Progress in Aerospace Sciences, 68, 1-26.
9. Yoshida, K., Nakanishi, H., Inaba, N., Ueno, H., & Oda, M. (2004). Contact dynamics and control strategy based on impedance matching for robotic capture of a non-cooperative satellite. In: Proc. of the 15th CISM-IFToMM Symp. On Robot Design, Dynamics and Control (ROMANSY), St-Hubert, Canada.
10. Wu, S., Mou, F., & Ma, O. (2017). Contact Dynamics and Control of a Space Manipulator Capturing a Rotating Object. In: Proc. of the AIAA Guidance, Navigation, and Control Conference (AIAA GNC), Grapevine, Texas, USA.
11. Van Vliet, J., Sharf, I., & Ma, O. (2000). Experimental validation of contact dynamics simulation of constrained robotic tasks. The International Journal of Robotics Research 19(12), 1203-1217.
12. Dexler, K. (1998). Nanosystems: Molecular Machinery, Manufacturing, and Computation, Wiley.
13. Rybus, T. & Seweryn, K. (2016). Planar air-bearing microgravity simulators: Review of applications, existing solutions and design parameters. Acta Astronautica 120, 239-259.
14. Colmenarejo, P., Avilés, M., & di Sotto, E. (2015). Active debris removal GNC challenges over design and required ground validation. CEAS Space Journal 7(2), 187-201.
15. Boge, T., Wimmer, T., Ma, O., & Zebenay, M. (2010). EPOS−A Robotics-Based Hardware-in-the-Loop Simulator for Simulating Satellite RvD Operations. In: Proc. of the 10th International Symposium on Artificial Intelligence, Robotics and Automation in Space (i-SAIRAS'2010), Sapporo, Japan.
16. Uyama, N., Fujii, Y., Nagaoka, K., & Yoshida, K. (2012). Experimental evaluation of contact-impact dynamics between a space robot with a compliant wrist and a free-flying object. In: Proc of the 11th International Symposium on Artificial Intelligence and Robotics and Automation in Space (i-SAIRAS'2012), Turin, Italy.
17. Kolvenbach, H. & Wormnes, K. (2016). Recent developments on ORBIT, a 3-DoF Free Floating Contact Dynamics Testbed. In: Proc of the 13th International Symposium on Artificial Intelligence and Robotics and Automation in Space (i-SAIRAS'2016), Beijing, China.
18. Zebenay, M., Lampariello, R., Boge, T., & Choukroun, D. (2012). A new contact dynamics model tool for hardware-in-the-loop docking simulation. In: Proc of the 11th International Symposium on Artificial Intelligence and Robotics and Automation in Space (i-SAIRAS'2012), Turin, Italy.
19. Liu, H., Liang, B., Xu, W., Di, Z., & Wang, X. (2012). A ground experiment system of a free-floating robot for fine manipulation. International Journal of Advanced Robotic Systems, 9(5).
20. Seweryn, K., Baran, J., Barciński, T., Colmenarejo, P., Łoś, A., et al. (2017). The prototype of space manipulator WMS LEMUR dedicated to capture tumbling satellites in on-orbit environment. In: Proc of the 11th International Workshop on Robot Motion and Control (RoMoCo'2017), Wąsowo, Poland.
21. Oleś, J., Kindracki, J., Rybus, T., Mężyk, Ł., Paszkiewicz, P., et al. (2017). A 2D Microgravity Test Bed for the Validation of Space Robot Control Algorithms. Journal of Automation, Mobile Robotics & Intelligent Systems 11(2), 81-90.
22. Wieser, M., Richard, H., Hausmann, G., Meyer,

J.C., Jaekel, S., et al, (2015). e.Deorbit Mission: OHB Debris Removal Concepts. In: Proc. of the 13th Symposium on Advanced Space Technologies in Robotics and Automation (ASTRA'2015), ESTEC, Noordwijk, The Netherlands.

23. Seweryn, K. & Banaszkiewicz, M. (2008). Optimization of the trajectory of a general free-flying manipulator during the rendezvous maneuver. In: Proc. AIAA-GNC'2008 conf., Honolulu, USA.
24. Rybus, T., Seweryn, K. & Sąsiadek, J.Z. (2017). Control system for free-floating space manipulator based on Nonlinear Model Predictive Control (NMPC). J. Intell. Robot. Syst., vol. 85(3), pp. 491-509.
25. Dubowsky, S. & Papadopoulos, E. (1993). The Kinematics, Dynamics and Control of Free-flying and Free-floating Space Robotic Systems. IEEE Transactions on Robotics and Automation 9 (5), 531-543.